Süleyman Demirel Üniversitesi Fen Edebiyat Fakültesi Fen Dergisi
Süleyman Demirel University Faculty of Arts and Sciences Journal of Science
2019, 14(2): 296–315
DOI: 10.29233/sdufeffd.572188
Atıf için / For Citation: A. GEDIZ ERTÜRK, "A Synthetic, Spectroscopic, Theoretical and Biological Perspective on a Novel Schiff Base Included 4-Aminoantipyrine", *Süleyman Demirel Üniversitesi Fen Edebiyat Fakültesi Fen Dergisi*, 14(2), 296–315, 2019.

A Synthetic, Spectroscopic, Theoretical and Biological Perspective on a Novel Schiff Base Included 4-Aminoantipyrine

Aliye GEDİZ ERTÜRK[*1]
[1]*Ordu Üniversitesi, Fen Edebiyat Fakültesi, Kimya Bölümü, 52200, Ordu, Türkiye*

**corresponding author e-mail: aliyeerturk@gmail.com*

(Alınış / Received: 30.05.2019, Kabul / Accepted: 30.09.2019, Yayımlanma / Published: 30.11.2019)

Abstract: A novel Schiff base, 4-(([1,1'-biphenyl]-4-ylmethylene)amino)-1,5-dimethyl-2-phenyl-1,2-dihydro-3*H*-pyrazol-3-one (BiPhAAP), obtained from biphenyl carboxaldehyde with 4-aminoantipyrine was characterized using elemental analysis, FT-IR, and ^{1}H and ^{13}C NMR spectroscopic methods. In addition to the spectroscopic findings, geometrical descriptions and the extent of surface interactions in the compound were determined by X-ray single crystallographic and Molecular Hirshfeld surface (MHS) analysis techniques. The distinctions between experimental and calculated FT-IR results have proved the presence of intra-molecular (C–H….O type) hydrogen bonds in the crystal structure. The in vitro antimicrobial potential, which was studied against two Gram-negative (*Escherichia coli* and *Proteus vulgaris*) and two Gram-positive (*Bacillus subtilis* and *Micrococcus luteus*) bacterial strains, and three yeast strains (*Candida albicans*, *Aspergillus niger* and *Candida globrata*) was examined by using the agar well diffusion method at concentrations of 250, 125 and 62.5 mg/mL. The in vitro antioxidant activities of this compound were estimated by five different antioxidant assays (DPPH radical scavenging, reducing power, metal chelating activity, superoxide scavenging, and total antioxidant). Cytotoxic activity of the new compound was sought against human breast carcinoma cells (MCF-7). The IC_{50} values were established with respect to the MTT test.

***Keywords**:* 4-Aminoantipyrine, Antimicrobial activity, Antioxidant activity, MTT assay, Theoretical study

4-Aminoantipirin İçeren Yeni Bir Schiff Baz Üzerine Sentetik, Spektroskopik, Teorik ve Biyolojik Açıdan Bir İnceleme

Özet: 4-Aminoantipirin ile bifenil karboksaldehitten yeni bir Schiff bazı olan 4-(([1,1'-bifenil]-4-ilmetilen)amino)-1,5-dimetil-2-fenil-1,2-dihidro-3*H*-pirazol-3-on (BiPhAAP) sentezlendi ve elementel analiz, FT-IR ve ^{1}H ve ^{13}C NMR spektroskopik metotları kullanılarak karakterize edildi. Spektroskopik bulgulara ek olarak, geometrik tanımlar ve bileşikteki yüzey etkileşimlerinin kapsamı X-ışını kristalografik ve Moleküler Hirshfeld yüzey (MHS) analizi teknikleriyle belirlenmiştir. Deneysel ve hesaplanan FT-IR sonuçları arasındaki farklar kristal yapısında molekül içi (C-H….O tipi) hidrojen bağlarının varlığını kanıtlamıştır. İki Gram negatif (*Escherichia coli* ve *Proteus vulgaris*) ve iki Gram pozitif (*Bacillus subtilis* ve *Micrococcus luteus*) bakteri suşu ve üç maya suşuna (*Candida albicans*, *Aspergillus niger* ve *Candida globra*) karşı çalışılan *in vitro* antimikrobiyal potansiyel 250, 125 ve 62.5 mg/mL konsantrasyonlarda agar well difüzyon metodu kullanılarak incelenmiştir. Bu bileşiğin *in vitro* antioksidan aktiviteleri, beş farklı antioksidan testi (DPPH radikal süpürme, indirgeme gücü, metal şelatlama etkinliği, süperoksit temizleme ve toplam antioksidan) ile hesaplandı. Yeni bileşiğin sitotoksik aktivitesi, insan meme kanseri hücrelerine (MCF-7) karşı araştırıldı. IC_{50} değerleri ise, MTT testine göre belirlendi.

Anahtar kelimeler: 4-Aminoantipirin, Antimikrobiyal aktivite, Antioksidan aktivite, MTT testi, Teorik çalışma

1. Introduction

Heterocyclic compounds are organic structures that contain two distinct elements as members of their ring(s). Replacement of one or more carbon atoms in their ring structure converts heterocyclic compounds into various analogs. They are ubiquitously found in all living organisms and have a wide variety of biological functions. These characteristics together make the heterocyclic compounds one of the most significant organic molecules. Many modern-day drugs contain a heterocyclic skeleton or a substituent. For example, pyrazolone is an N-heterocyclic compound commonly used in drug design. Furthermore, heterocyclic compounds increase drug efficacy especially when acts as a chelating agent. 4-aminoantipyrine (4-AAP) is a highly bioactive member of the pyrazolone family. Its efficacy has been shown to increase in Schiff base systems, improving its potential as a bioactive carbonyl compound (aldehydes and ketones). This increase in biopotency is further enriched by a wide range of complex compounds produced by various transition metals [1]. For example, Schiff bases derived from 4-aminoantipyrine caused increased cytotoxicity in cancerous MCF-7 breast epithelial cell line when compared to the standard drug, Doxorubicin [2]. Their vanillin derivatives and metal complexes showed satisfying antibacterial activity, while their isatine derivatives showed notable antimicrobial and antioxidant activity [3]. It was revealed that Schiff base compounds derived from 4-AAP had analgetic [4], antihelmintic [5], analgesic, and antipyretic effects [6] as well as promising new kinds of chemo-therapeutic antitumor agent attributes [7]. Moreover, they enabled the determination of liver disease during the clinical treatment process [8].

We synthesized and characterized BiPhAAP, a novel heterocyclic compound by using FT-IR, ^{1}H-NMR, ^{13}C-NMR spectroscopies, elemental, single-crystal X-ray diffraction, and quantum chemical analysis. Through the MHS analysis, various intermolecular interactions and crystal packaging in the crystal structure of BiPhAAP were mapped via electrostatic potential [9]. We characterized the potential biological activities of this novel Schiff base compound derived from 4-AAP by testing its antibacterial, antifungal, and cytotoxic properties as well as its antioxidant properties on activities by various methods. The cytotoxic effects of BiPhAAP were investigated on MCF-7 breast carcinoma cells by measuring cell viability [10]. In vitro antimicrobial activities were measured by using Gram (+) bacteria (*M. luteus*, *B. subtilis*), Gram (-) bacteria (*P. vulgaris*, *E. coli*) and yeast (*A. niger*, *C. albicans*, *C. glabrata*) by using agar well diffusion values [11]. In vitro, antioxidant tests were used to measure the effects of BiPhAAP on oxidative stress. Antioxidant supplements purify the organism from free radicals and active oxygen species in chain reactions. That is, antioxidants are inhibitors that greatly reduce oxidative damage [12, 13]. For this purpose, we used five different methods to determine the antioxidant properties of the compound (**3**). Following this we compared its capacity with known synthetic antioxidants e.g. BHA, BHT, EDTA, Trolox, Resorcinol, and α-tocopherol.

2. Material and Method

All chemicals and solvents were procured as reagent grade from Sigma-Aldrich or Merck and they were used without further purification. The IR spectrum was recorded using on a Shimadzu IR Affinity-1. ATR-FT-IR spectrophotometer with the frequency range of 4000–400 cm^{-1}. ^{1}H and ^{13}C NMR spectra were measured using a Varian 400

MHz (^{1}H) or 100 MHz (^{13}C) NMR Spectrometer. Chemical shifts (δ) are reported in ppm and were referenced to residual DMSO-d_6 (δ 2.50 ppm for ^{1}H NMR and δ 39.51 ppm for ^{13}C NMR) as the internal standard. Elemental analyses were performed with an Elementar Vario Micro Cube elemental analyzer at ODUMARAL (Ordu University). MTT and antioxidant assays absorbances were measured in Biotek (USA) microplate reader. Standard procedures to minimize the variation (triplicates averaged) and repetition (three times) was used to assure accuracy and repeatability.

2.1 Synthesis of BiPhAAP (3)

After biphenyl-4-carbaldehyde (**2**) (1000 mg, 5.49 mmol) was dissolved in 15 mL of absolute ethanol, 2 drops of glacial acetic acid were added.

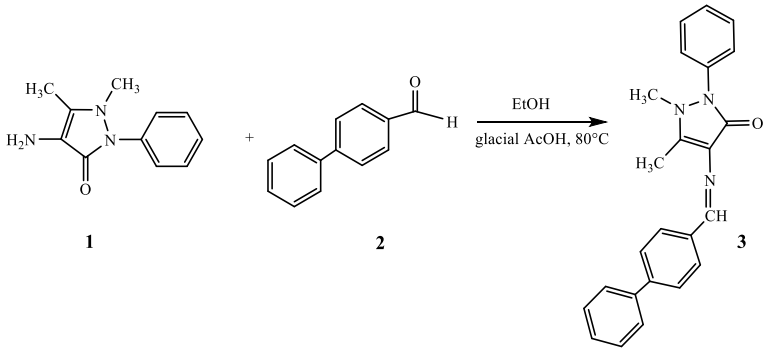

Figure 1. Synthesis pathway of BiPhAAP

4-AAP (**1**) (1120 mg, 5.49 mmol) dissolved in 10 mL anhydrous ethyl alcohol was added to the mixture. The solution was refluxed for 11 hours (Figure 1) during which, it was monitored by thin layer chromatography in a 5:2 ethyl acetate:hexane solvent system (R_f: 0.85). A pale yellow solid precipitate formed as a result of the condensation reaction. The resulting mixture was filtered to catch the precipitate. The precipitate was washed successively with ethanol and diethyl ether. The resulting solids were crystallized from 2-propanol. Bright lemon yellow needle-shaped solids (**3**) were obtained. Yield: 84%, MP: 192-193 °C. **FT-IR** (ATR, ν, cm^{-1}): 3055-3028 (aromatic =C-H), 2939 (aliphatic C-H), 1639 (C=O), 1593 (C=N), 1558-1458 (aromatic C=C). **^{1}H-NMR** (DMSO-d_6, 400 MHz, δ, ppm): 9.64 (s, 1H, -N=CH), 7.91 (d, 2H, *J*: 8.1 Hz, biphenyl-CH) 7.78 (d, 2H, *J*: 8.1 Hz, biphenyl-CH), 7.74 (d, 2H, *J*: 7.7 Hz, 2.ring of biphenyl group-CH), 7.57-7.48 (m, 4H, biphenyl ring), 7.42-7.39 (m, 4H, antipyrine phenyl ring), 3.20 (s, 3H pyrazolone N-CH_3), 2.49 (s, 3H, pyrazolone C-CH_3). **^{13}C-NMR** (DMSO-d_6, 100 MHz, δ, ppm): 160.07 (C=O), 154.21 (HC=N), 152.66 (C=C), 142.10, 139.95 (2C), 137.13, 135.03, 129.63 (2C), 129.50 (2C), 128.28 (2C), 127.46 (2C), 127.41 (2C), 127.16 (2C), 125.07, 116.86, 35.81 (N-CH_3), 10.25 (C-CH_3). Anal. Calcd for $C_{24}H_{21}N_3O$ (%): C, 78.45; H, 5.76; N, 11.44. Found (%): C, 77.48; H, 5.85; N, 11.29.

2.2 X-ray diffraction study

A selected crystal with bright lemon yellow color and sizes of 0.560 x 0.330 x 0.040 mm was placed on X-ray diffractometer (STOE IPDS II). X-ray data were obtained at room temperature (293 K) using graphite monochromated Mo Kα radiation (k = 0.71073 A). The cell parameters were designated by using X-AREA software. Following this, X-RED32 software was used to calculate the absorption correction (μ = 0.09 mm^{-1}) [14]. SHELXS-97 program, by using direct methods, was used when analyzing the crystal structure. That ensured scattering factors [15]. The molecular plot

was generated by using ORTEPIII for Windows [16]. We used the WinGX software to prepare this manuscript for publication [17]. Table 1 summarizes the data collection conditions and the refinement parameters. CCDC deposit number is 1941768.

2.3 Molecular Hirshfeld surface analysis

The MHS computations were prepared by using the CRYSTALEXPLORER [18] which determined the bond lengths to hydrogen by using the cif file of BiPhAAP. The program settings allowed all values to be modified to the standard neutron values (C-H= 1.083 Å) automatically. The 2D fingerprint plots were prepared by using the standard 0.6–2.6 Å aspect. The graph axes include the *de* and *di* distance scales.

Table 1. Crystallographic data and structure refinement parameters for $C_{24}H_{21}N_3O_1$

$C_{24}H_{21}N_3O_1$	STOE *IPDS* 2 Diffractometer
M_W= 367.44	Mo *K*α radiation
Triclinic, *P*1	V= 987.5 (9) Å^3
T= 293 K	Z= 2
a= 7.126 (3) Å	0.56 × 0.33 × 0.04 mm
b= 9.446 (5) Å	4002 reflections
c= 15.100 (8) Å	255 parameters
α= 85.15 (4)°	$\Delta\rho_{max}$= 0.14 e Å^{-3}
β= 79.74 (4)°	$\Delta\rho_{min}$= −0.15 e Å^{-3}
γ= 81.53 (4)°	$R[F^2 > 2\sigma(F^2)]$= 0.064
μ= 0.09 mm^{-1}	$wR(F^2)$= 0.135
11819 measured reflections	S= 0.98
4002 independent reflections	T_{min}= 0.965; T_{max}= 0.996
1917 observed reflections [$I > 2\sigma(I)$]	$(\sin\theta/\lambda)_{max}$= 0.628 Å^{-1}
R_{int}= 0.071	Absorption correction= Integration

Computer programs: STOE *X-AREA*, STOE *X-RED*, *SHELXL2016*/6 (Sheldrick, 2016).

2.4 In vitro antibacterial and antifungal activity

The stock solutions of BiPhAAP and the positive control (Ampicillin) were prepared in DMSO. Two Gram(-) (*E. coli* ATTC 25922 and *P. vulgaris* ATCC®7829*)* and two Gram(+) (*B. subtilis* B209 and *M. luteus* B1018) bacterial strains were used to test the antibacterial activity. Antifungal activities of compound (**3**) were tested against three fungal cultures, *C. albicans* ATCC®10231, *A. niger* ATCC®9642 and *C. globrata* ATCC 66032. Antifungal drug Nystatin was used as the positive control. The bacterial strains and yeast cultures (curtesy of Ordu University, Microbiology Laboratory, Ordu, Turkey) were maintained under standard conditions. The antibacterial and the antifungal properties of the compound (**3**) were measured by using the agar well diffusion method [19]. All cultures at T_0 contained approximately 5x10^5 colony forming units (CFU)/mL. The bacterial and fungal cultures were treated with 250, 125 & 62.5 mg/mL concentrations of compound (**3**) dissolved in DMSO. Using a sterile cork borer (5 mm in diameter) wells were made in each agar plate, more than 0.1 mL of the BiPhAAP solutions was poured into three wells, and the four bacterial strains and the three yeasts in the dishes were maintained under standard conditions (37°C) for 24 h and for 48 h, respectively. Ampicillin and Nystatin (positive controls for bacteria and yeast respectively) were used for comparison under similar conditions. DMSO, used as the vehicle to dissolve compound **(3)**, was used as the negative control. The growth of the microorganisms was inhibited by diffusion of the test solutions. Percentages of

inhibition zones were used to evaluate bactericidal and fungicidal capacity [20]. The means of zones of inhibition (mm) was compared with that of positive controls. The results were exhibited as the mean ± standard deviation (SD).

2.5 Antioxidant activity

The percent activities of radical inhibition of the BiPhAAP for all antioxidant assays was calculated by using the following equation (1):

$$Activity\ (\%) = [1 - \left(\frac{A_{sample}}{A_{control}}\right)] \times 100 \quad (1)$$

2.5.1 DPPH free radical scavenging activity

Free radical scavenging capacity of BiPhAAP was evaluated based on the compound's ability to reduce 1,1-diphenyl-2-picrylhydrazyl (DPPH)-free radical as described by Brand-Williams et al. [21] with minor modifications. Varying concentrations (25, 50, 100, 200 and 400 µg/mL) of 0.5 mL BiPhAAP, and the antioxidant standards BHT, Trolox, and Resorcinol (5, 25, 50, 100, 200 and 400 µg/mL) was mixed with 3 mL of ethanol. 0.3 mL of 0.25 mM DPPH solution (prepared in ethanol) was added to these solutions. After shaking vigorously the solution was incubated in dark at room temperature for 60 min. The absorbance of the samples (A) was quantified at 517 nm against ethanol blank. The control test was made with the ethanol and DPPH solution.

2.5.2 The reducing power

This activity was determined according to Oyaizu [22]. The absorbance of the solution was quantified at 700 nm. The control was obtained in a similar way short of the samples. The blank sample consisted of TCA, $FeCl_3$, and water. EDTA and Trolox were used as standards.

2.5.3 Metal chelating activity

The ferrous ion (Fe^{2+}) chelating activities of the BiPhAAP determined according to Decker and Welch [23] by using BHT, EDTA, and Trolox as standards. The absorbance of the solution was quantified at 562 nm against $FeCl_2$ and water blank. All trials were repeated in triplicate and averaged.

2.5.4 Superoxide scavenging activity

The superoxide anion scavenging activity of the BiPhAAP compound was calculated according to Liu et al. [24]. The absorbance was measured at 560 nm against water as the blank. The control contained all reagents, except the sample. BHA, BHT, and Trolox were used as standards.

2.5.5 Total antioxidant activity

The total antioxidant activity of BiPhAAP was tested by using the ferric thiocyanate method (FTC) by Chang et al. [25]. The peroxide level of lipid peroxidation of solutions was measured by using spectrophotometer at 500 nm against the control. The absorbance was measured every 6 h until the control reached saturation. BHT,

Resorcinol and Ascorbic acid were used as standards. The control contained all reagents, except the sample.

2.6 Cytotoxicity analysis

2.6.1 Cell culture and MTT assay

The human breast cancer cell line, MCF-7 (ATCC® HTB-22™), was maintained according the ATCC protocol. Cultures were kept in CO_2 incubator at 37 °C under 5% CO_2. Cells were maintained in EMEM supplemented with 10% FBS and 1% penicillin/streptomycin. Cell viability was measured using the standard MTT cell viability assay [26, 27]. MCF-7 cells were dislodged from the culture flasks using trypsin/EDTA. Cells were cultured into 96 well plate in standard medium at 1×10^4 cells per well and cultured overnight. To measure viability various concentrations of BiPhAAP (0-30 mM) were added to on to the cells. BiPhAAP was dissolved in DMSO and diluted in distilled water. DMSO concentration in the treatment solutions were kept to a minimum (0.1% of total culture medium volume). Control group received the same treatment, except BiPhAAP. Cells were cultured in their corresponding medium for 24, 48 and 72 h. At the end of the respective treatment times MTT solution (5 mg/mL) was added to each well and the cells were further incubated for 4 h in the CO_2 incubator. Then the medium was removed without disturbing the cells. DMSO (100 μL) was added to solubilize formazan crystals formed by MTT reduction in living cells. Spectrophotometric measurements were recorded at 570 nm by using a microplate reader. The following equation was used to determine the percentage of viable cells (2):

$$Cell\ Viability\ (\%) = \frac{A_{Sample}}{A_{Control}} \times 100 \quad (2)$$

IC_{50} (the concentration which inhibits or kills 50% of the total cells) were calculated by using non-linear regression analysis.

3. Results

3.1 Computational procedure

The quantum-chemical procedure was used to predict the structure of the title chemical. Computational data were compared with the data obtained from experiments. The Gaussian 03 software package was used to construct the optimized molecular structure. Both *ab* initio Hartree–Fock (HF) and density functional theory DFT (B3LYP) methods using the 6-31 + G(d) basis set [28-31]. Gaussian 03 program [32, 33] was utilized for theoretical calculations. Bond lengths values were calculated as 0.021171 and 0.043354. The attachment angles values were found to be 1.168175 and 1.634573 (Table 2). When we compared the results obtained from B3LYP data with the experimental data by using RMSE method. The theoretical outcomes were found to be compatible with the experimental crystallographic outcomes. A drawing of the crystal structure of BiPhAAP was generated by using Ortep-3 (Figure 2a). BiPhAAP crystallizes in the triclinic space group *P*1 with Z= 2. Hydrogen bonds provide stability to the crystal structure. The packing diagram of the crystal is shown in Figure 2b.

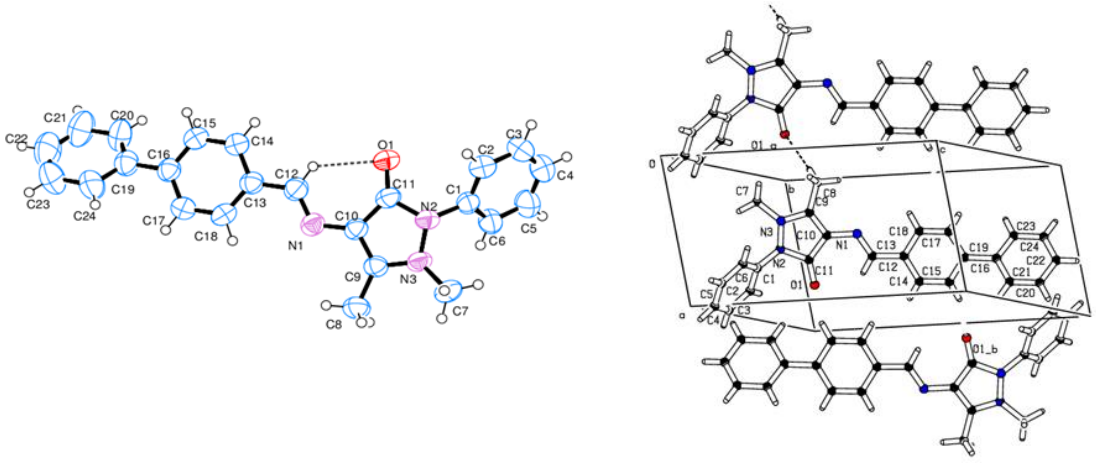

(a) (b)

Figure 2. (a) Ortep-3 diagram (Displacement ellipsoids are drawn at the 30% probability level and H atoms are displayed as small spheres of arbitrary radii); **(b)** Packing diagram of the BiPhAAP

Table 2. Molecular structure parameters for BiPhAAP

Parameter	Experimental	DFT	HF
Bond Length (A°)			
O_1-C_{11}	1.226 (3)	1.2289	1.203
N_3-C_9	1.357 (3)	1.387	1.3887
N_3-N_2	1.403 (3)	1.4133	1.4023
N_3-C_7	1.457 (3)	1.4687	1.46
N_2-C_{11}	1.410 (3)	1.4159	1.3828
N_2-C_1	1.433 (3)	1.4225	1.422
N_1-C_{12}	1.277 (3)	1.2913	1.262
N_1-C_{10}	1.393 (3)	1.3835	1.3897
C_{11}-C_{10}	1.436 (4)	1.4683	1.4679
C_9-C_{10}	1.366 (4)	1.3741	1.3431
C_9-C_8	1.481 (4)	1.492	1.4937
C_1-C_2	1.369 (4)	1.4014	1.3881
C_1-C_6	1.379 (4)	1.4019	1.3883
C_{13}-C_{18}	1.379 (4)	1.4077	1.3949
C_{13}-C_{14}	1.386 (4)	1.4056	1.3895
C_{13}-C_{12}	1.460 (4)	1.4656	1.4765
C_{16}-C_{15}	1.380 (4)	1.4058	1.3907
C_{16}-C_{17}	1.391 (4)	1.4105	1.3983
C_{16}-C_{19}	1.485 (4)	1.4849	1.4909
C_{19}-C_{20}	1.380 (5)	1.407	1.394
C_{19}-C_{24}	1.384 (5)	1.407	1.394
C_{14}-C_{15}	1.380 (4)	1.3933	1.3873
C_6-C_5	1.380 (4)	1.3965	1.3874
C_{18}-C_{17}	1.374 (4)	1.3894	1.3806
C_2-C_3	1.391 (5)	1.3956	1.3856
C_3-C_4	1.372 (5)	1.3982	1.3877
C_{20}-C_{21}	1.382 (5)	1.3958	1.3867
C_5-C_4	1.353 (5)	1.3973	1.3862
C_{24}-C_{23}	1.380 (5)	1.3958	1.3866
C_{21}-C_{22}	1.360 (6)	1.3979	1.387
C_{22}-C_{23}	1.371 (6)	1.3979	1.3871
RMSE		0,021171	0,043354
Parameter	**Experimental**	**DFT**	**HF**
***Bond Angle* (°)**			

C_9-N_3-N_2	107.6 (2)	106.685	105.674
C_9-N_3-C_7	124.5 (2)	119.4701	117.2881
N_2-N_3-C_7	117.6 (2)	114.3264	112.3437
N_3-N_2-C_{11}	108.7 (2)	109.6964	110.214
N_3-N_2-C_1	119.0 (2)	118.9356	118.2532
C_{11}-N_2-C_1	121.6 (2)	123.8039	122.6833
C_{12}-N_1-C_{10}	120.3 (3)	121.0021	121.4396
O_1-C_{11}-N_2	122.9 (3)	124.3198	124.8222
O_1-C_{11}-C_{10}	132.2 (3)	130.8398	130.0627
N_2-C_{11}-C_{10}	104.8 (2)	104.813	105.1025
N_3-C_9-C_{10}	110.1 (2)	110.7966	111.4295
N_3-C_9-C_8	120.8 (2)	121.3729	120.4348
C_{10}-C_9-C_8	129.1 (3)	127.8275	128.1346
C_9-C_{10}-N_1	122.7 (3)	123.2319	123.8659
C_9-C_{10}-C_{11}	108.3 (2)	107.5829	107.0777
N_1-C_{10}-C_{11}	128.8 (2)	129.1359	128.9958
C_2-C_1-C_6	120.7 (3)	120.16	120.1778
C_2-C_1-N_2	118.9 (3)	118.8194	118.8689
C_6-C_1-N_2	120.3 (3)	121.0186	120.9534
C_{18}-C_{13}-C_{14}	117.4 (3)	118.2125	118.5298
C_{18}-C_{13}-C_{12}	122.2 (3)	122.6257	122.3855
C_{14}-C_{13}-C_{12}	120.4 (3)	119.1617	119.0847
N_1-C_{12}-C_{13}	122.4 (3)	121.8242	121.8229
C_{15}-C_{16}-C_{17}	117.2 (3)	117.8216	118.1951
C_{15}-C_{16}-C_{19}	120.9 (3)	121.1454	120.9789
C_1-C_{16}-C_{19}	121.9 (3)	121.0331	120.826
C_{20}-C_{19}-C_{24}	117.5 (3)	118.0677	118.3783
C_{20}-C_{19}-C_{16}	121.5 (3)	120.9851	120.8201
C_{24}-C_{19}-C_{16}	120.9 (3)	120.9471	120.8016
C_{15}-C_{14}-C_{13}	121.3 (3)	121.0224	120.9326
C_1-C_6-C_5	118.6 (3)	119.7146	119.7088
C_1-C_2-C_3	119.4 (3)	119.5103	119.6876
C_{14}-C_{15}-C_{16}	121.3 (3)	120.9509	120.7045
C_{17}-C_{18}-C_{13}	121.5 (3)	120.6677	120.5251
C_{18}-C_{17}-C_{16}	121.3 (3)	121.3249	121.1128
C_4-C_3-C_2	119.9 (4)	120.6725	120.4897
C_{19}-C_{20}-C_{21}	121.2 (4)	120.9882	120.8358
C_4-C_5-C_6	121.5 (4)	121.5019	120.4112
C_5-C_4-C_3	119.8 (4)	119.5	119.5159
C_{23}-C_{24}-C_{19}	121.0 (4)	120.9879	120.8378
C_{22}-C_{21}-C_{20}	120.5 (4)	120.2709	120.2488
C_{21}-C_{22}-C_{23}	119.3 (4)	119.4151	119.4525
C_{22}-C_{23}-C_{24}	120.4 (4)	120.2701	120.2467
RMSE		1,168175	1,634573
Parameter	**Experimental**	**DFT**	**HF**
Torsion Angle (°)			
C_9-N_3-N_2-C_{11}	−7.7 (3)	-6.7922	-7.3476
C_7-N_3-N_2-C_{11}	−154.4 (2)	-141.1498	-136.4092
C_9-N_3-N_2-C_1	−152.8 (2)	-157.6159	-155.6828
C_7-N_3-N_2-C_1	60.6 (3)	68.0265	75.2556
N_3-N_2-C_{11}-O_1	−172.0 (2)	-173.1311	-172.4077
C_1-N_2-C_{11}-O_1	−28.1 (4)	-24.0244	-25.7333
N_3-N_2-C_{11}-C_{10}	5.6 (3)	5.1439	6.4118
C_1-N_2-C_{11}-C_{10}	149.5 (3)	154.2507	153.0863

N_2-N_3-C_9-C_{10}	6.8 (3)	137.3367	131.4642
C_7-N_3-C_9-C_{10}	150.6 (3)	5.783	5.3752
N_2-N_3-C_9-C_8	−171.5 (2)	-173.6277	-174.9847
C_7-N_3-C_9-C_8	−27.7 (4)	-42.0739	-48.8957
N_3-C_9-C_{10}-N_1	172.9 (2)	175.0391	175.8851
C_8-C_9-C_{10}-N_1	−9.0 (4)	-5.5979	-3.7203
N_3-C_9-C_{10}-C_{11}	−3.3 (3)	-2.6169	-1.5081
C_8-C_9-C_{10}-C_{11}	174.8 (3)	176.7461	178.8865
C_{12}-N_1-C_{10}-C_9	−178.7 (3)	178.3273	179.5338
C_{12}-N_1-C_{10}-C_{11}	−3.4 (4)	-4.5539	-3.673
O_1-C_{11}-C_{10}-C_9	175.8 (3)	176.5297	175.7191
N_2-C_{11}-C_{10}-C_9	−1.5 (3)	-1.5872	-3.0147
O_1-C_{11}-C_{10}-N_1	0.0 (5)	-0.9425	-1.4957
N_2-C_{11}-C_{10}-N_1	−177.3 (2)	-179.0593	179.7705
N_3-N_2-C_1-C_2	−157.6 (2)	-155.9713	-150.87
C_{11}-N_2-C_1-C_2	62.0 (4)	57.5573	64.9532
N_3-N_2-C_1-C_6	25.9 (4)	24.5357	29.1057
C_{11}-N_2-C_1-C_6	−114.5 (3)	-121.9357	-115.0711
C_{10}-N_1-C_{12}-C_{13}	177.7 (2)	179.7681	-179.9462
C_{18}-C_{13}-C_{12}-N_1	7.5 (4)	-0.1785	0.3362
C_{14}-C_{13}-C_{12}-N_1	−172.2 (3)	179.9085	-179.6302
C_{15}-C_{16}-C_{19}-C_{20}	38.4 (5)	38.7018	45.7045
C_{17}-C_{16}-C_{19}-C_{20}	−143.0 (3)	-141.2849	-134.2882
C_{15}-C_{16}-C_{19}-C_{24}	−140.4 (3)	-141.2849	-134.2685
C_{17}-C_{16}-C_{19}-C_{24}	38.1 (5)	38.7284	45.7389
C_{18}-C_{13}-C_{14}-C_{15}	−1.5 (4)	0.0627	0.0263
C_{12}-C_{13}-C_{14}-C_{15}	178.2 (3)	179.9796	179.9941
C_2-C_1-C_6-C_5	0.4 (4)	0.7708	0.3365
N_2-C_1-C_6-C_5	176.8 (3)	-179.7429	-179.6389
C_{13}-C_{14}-C_{15}-C_{16}	−1.3 (5)	-0.0223	0.0076
C_{17}-C_{16}-C_{15}-C_{14}	3.0 (4)	-0.0208	-0.015
C_{19}-C_{16}-C_{15}-C_{14}	−178.4 (3)	179.9921	179.9921
C_{14}-C_{13}-C_{18}-C_{17}	2.6 (4)	-0.0607	-0.053
C_{12}-C_{13}-C_{18}-C_{17}	−177.1 (3)	-179.9745	179.9804
C_6-C_1-C_2-C_3	0.2 (4)	0.2416	0.5478
N_2-C_1-C_2-C_3	−176.3 (3)	-179.256	-179.4763
C_{13}-C_{18}-C_{17}-C_{16}	−0.9 (5)	0.0186	0.0465
C_{15}-C_{16}-C_{17}-C_{18}	−1.9 (5)	0.0226	-0.0119
C_{19}-C_{16}-C_{17}-C_{18}	179.5 (3)	-179.9903	179.981
C_1-C_2-C_3-C4	0.3 (5)	-0.9927	-0.9872
C_{24}-C_{19}-C_{20}-C_{21}	−0.5 (6)	0.0414	0.0189
C_{16}-C_{19}-C_{20}-C_{21}	−179.4 (3)	-179.9456	-179.9546
C_1-C_6-C_5-C_4	−1.4 (5)	-1.0471	-0.7934
C_6-C_5-C_4-C_3	1.8 (5)	0.3064	0.3601
C_2-C_3-C_4-C_5	−1.3 (5)	0.7218	0.5348
C_{20}-C_{19}-C_{24}-C_{23}	−0.3 (6)	-0.0529	-0.069
C_{16}-C_{19}-C_{24}-C_{23}	178.6 (4)	179.9342	179.9046
C_{19}-C_{20}-C_{21}-C_{22}	0.1 (7)	-0.0105	0.0288
C_{20}-C_{21}-C_{22}-C_{23}	1.2 (7)	-0.0103	-0.0271
C_{21}-C_{22}-C_{23}-C_{24}	−2.0 (7)	-0.0011	-0.0226
C_{19}-C_{24}-C_{23}-C_{22}	1.5 (7)	0.0334	0.0716

3.2 Hirshfeld surface analysis

MHS analysis was used to examine the intermolecular interactions within the synthesized compound by using Crystal-Explorer [34]. The d_e, d_i, and d_{norm}, surfaces were mapped over the normal range (Figure 3a). Red reigions represent the intermolecular and interatomic forces caused by strong hydrogen bonding [35], thus shows the C-H···O hydrogen bonds in the BiPhAAP. A fixed color scale of -0.2156 (red) to 1.3214 (blue) a.u. was used when d_{norm} was mapped over. In this figure red regions signify donor-acceptor interactions [36-38]. The two-dimensional (2D) fingerprint plots show the overall interactions contributing to the molecular structure in normal mode (Figure 3b). In our structure, H...H / H...H interactions are one of the most significant contributors (56.6%) of the overall crystal packing (Figure 4). Following these C ··· H / H ··· C interactions contribute to 26.5% whereas O ··· H / H ··· O interactions contribute 6.0%, and finally N ··· H / H ··· N contributes 3.6% to the overall crystal packing.

Figure 5a shows the views of the three-dimensional (3D) BiPhAAP MHS graphed over the electrostatic potential energy in the space -0.081 to 0.056 a.u. These were generated by using the STO-3G basis set at the Hartree–Fock level of theory. In Figure 5b, the 6-30 + G (d) basis set of the DFT / B3LYP theory and the MEP Map are drawn in the range of -0.062 to 0.034, and bondability can be determined by utilizing the electrostatic potential energy surfaces drawn by both base sets and programs.

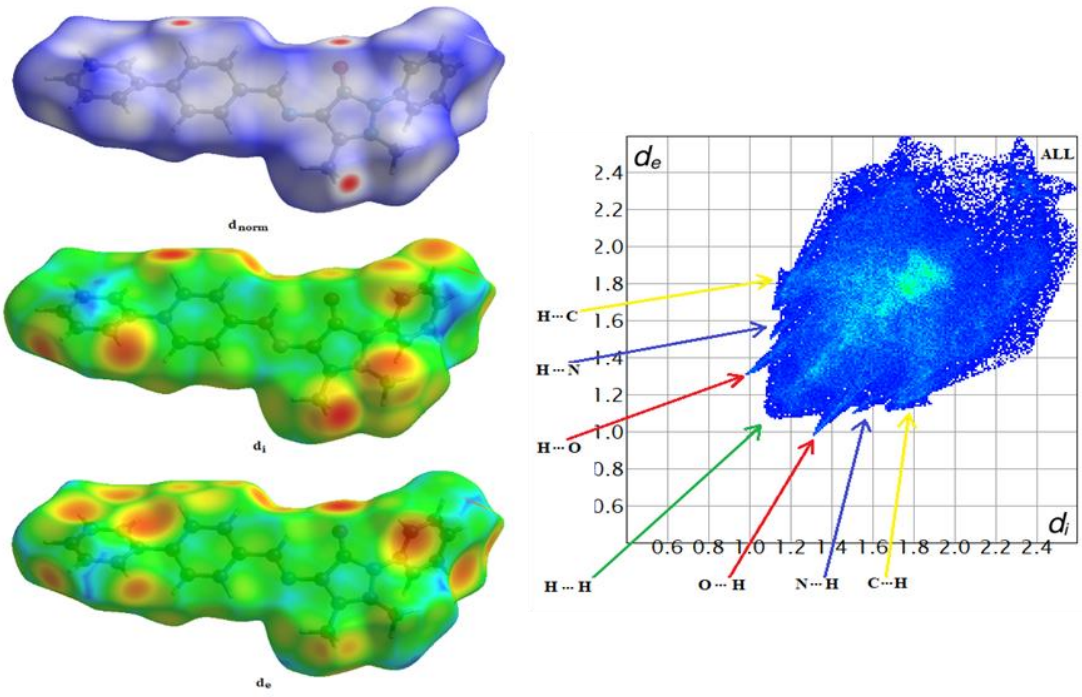

(a) (b)

Figure 3. (a) MHS of the BiPhAAP mapped over d_{norm}, d_i, and d_e **(b)** Fingerprint plot for the BiPhAAP

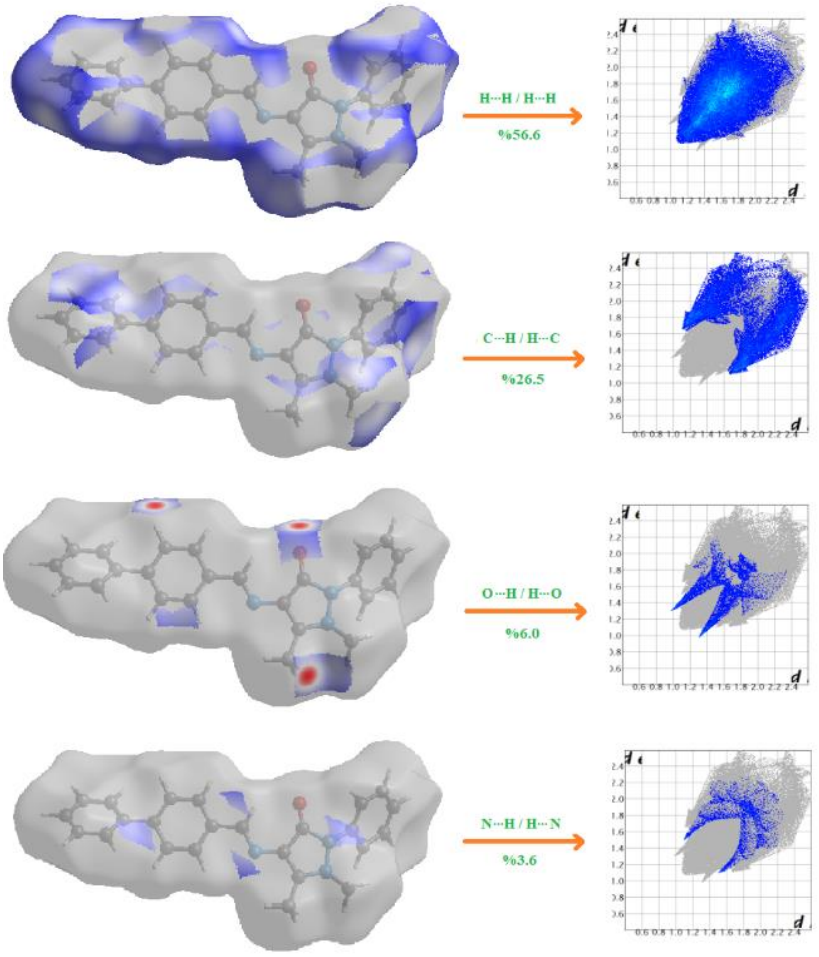

Figure 4. 2D fingerprint graphs with a d_{norm} view for the H···H (56.6%),C···H/H···C (26.5%), O···H/H···O (6.0%) and N···H/H···N (3.6%) interactions in the BiPhAAP

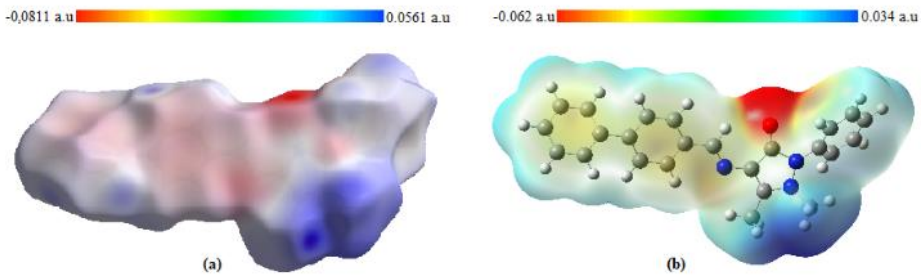

Figure 5. (a) The view of the 3D MHS of the BiPhAAP graphed over the electrostatic potential energy; **(b)** Molecular electrostatic potential map quantified at B3LYP/6–31+G(d) level

3.3 FT-IR spectrum

The infrared spectrum showed that BiPhAAP was formed as a result of a condensation reaction. This result is deduced from the fact that the occurrence of the characteristic stretching frequency of the azomethine bond (C=N) at 1593 cm^{-1} and no stretching bands of both the aminoantipyrine N-H and the aldehyde carbonyl (C = O) groups are present. The peak observed at 3275 cm^{-1} is the overtone peak for the compound [39].

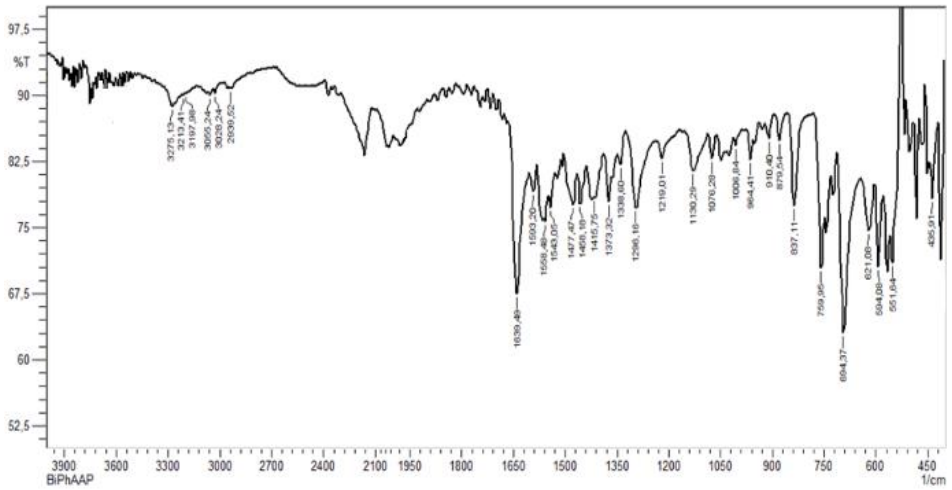

Figure 6. The FT-IR spectrum of BiPhAAP

As seen in Table 3, when the vibrational frequencies calculated from computational analysis and the experimental data are compared, the harmonic vibrational frequencies found to be higher than the experimental ones. We speculate that there are three reasons for this discrepancy; (1) insufficient size of basis set. When basis set is not used or its size is insufficient theoretical frequencies are found to be consistently higher than the experimental frequencies, (2) the neglect of electron correlation, and (3) the omission of anharmonicity [42]. We also speculate that the discrepancy seen in the stretching vibration of the C = O group (32 cm^{-1}) is a result of the C–H……O intramolecular hydrogen bond in the molecular structure of BiPhAAP. Our data show that the structure of our compound is consistent with similar Schiff base structures [43].

Table 3 Comparison of the experimental and theoretical vibrational frequencies (cm^{-1}) for BiPhAAP

Assignments	Experimental	Theoretical (Scaled)	
		B3LYP/6-31G (d)	HF/6-31G (d)
$\bar{\upsilon}_{aromatic}$ (C–H)	3055-3028	3092-3049	3046-2994
$\bar{\upsilon}_{alifatik}$ (C–H)	2939	3015-2923	2974-2858
$\bar{\upsilon}_{s}$ (C=O)	1639	1671	1710
$\bar{\upsilon}_{as}$ (C=N)	1593	1605	1677
$\bar{\upsilon}_{aromatic}$ (C=C)	1558-1458	1573-1477	1632-1557

3.4 NMR spectra

The molecular structure of BiPhAAP was analyzed by using the ^{1}H and ^{13}C NMR spectra. The presence of BiPhAAP in the molecular structure was confirmed by the lack of the peaks of the amine group of antipyrine and the aldehyde group of 9-biphenyl carbaldehyde as well as the presence of a peak for the azomethine group. In the spectrum, an azomethine proton (CH=N) is observed at 9·64 ppm (s, 1H). Biphenyl ring protons adjacent to the azomethine bond resonate at 7.91 ppm (d, *J*= 8.8 Hz, 2H) and 7.78 ppm (d, *J*= 8.6 Hz, 2H). At the end of the biphenyl group, phenyl ring protons are present (Figure 7). Chemical shift values for these protons are found to be in the range of 7.79-7.70 ppm (m, 5H). Additionally; the phenyl protons of the antipyrine ring are found to be at 7.42-7.39 ppm (m, 5H). Similar to the other antipyrine-based Schiff base compounds, ($N–CH_3$) methyl protons to nitrogen bound in the antipyrine ring are assigned at 3.20 ppm (s, 3H), and the ($=C–CH_3$) methyl protons to ethylenic carbon bound in the antipyrine ring are designated at 2.49 ppm (s, 3H) [44, 45].

The ^{13}C NMR spectrum is shown in Figure 8. According to the spectrum, the total quantity of the carbon peaks did not match well with the constitution of BiPhAAP but it did verify the formation of BiPhAAP. The ^{13}C NMR spectrum of BiPhAAP we detected an azomethine (C=N) peak at 154.21 ppm and a carbonyl (C=O) peak occurring at 160.07 ppm. We assigned the signal observed at 152.66 to (CH_3-**C**=) C9 of the ethylenic group to the antipyrine ring.

The aromatic region of the ^{13}C spectrum for BiPhAAP contained 13 peaks. The number of observed peaks does not match the expected 20 carbon peaks, six for quaternary carbons and fourteen for aromatic –CH carbons. Quaternary carbons are especially difficult to recognize since they have long relaxation times, therefore often they are not observable when all other signals are present. Because aromatic –CH carbons have also similar chemical parameters, they might resonate at the same time and frequency. We speculate that seven of the thirteen peaks have higher intensities (double-weight peak) therefore they correspond to fourteen aromatic –CH carbon [46]. While the peak at 35.81 ppm belongs to the nitrogen 3-bound methyl (N-CH_3) in the antipyrine ring, the peak at 10.25 ppm belongs to the ring C9-bound methyl (=C-**C**H_3) in the antipyrine ring [47].

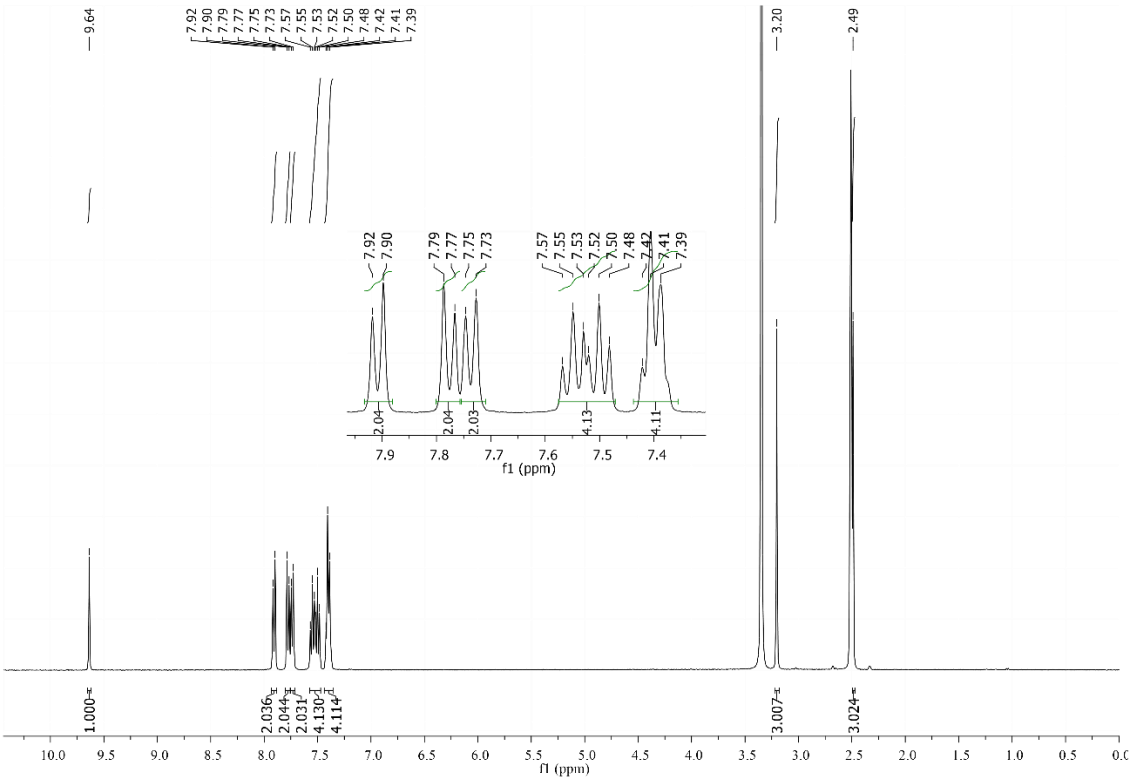

Figure 7 The ^{1}H NMR spectrum in DMSO-d_6 of BiPhAAP

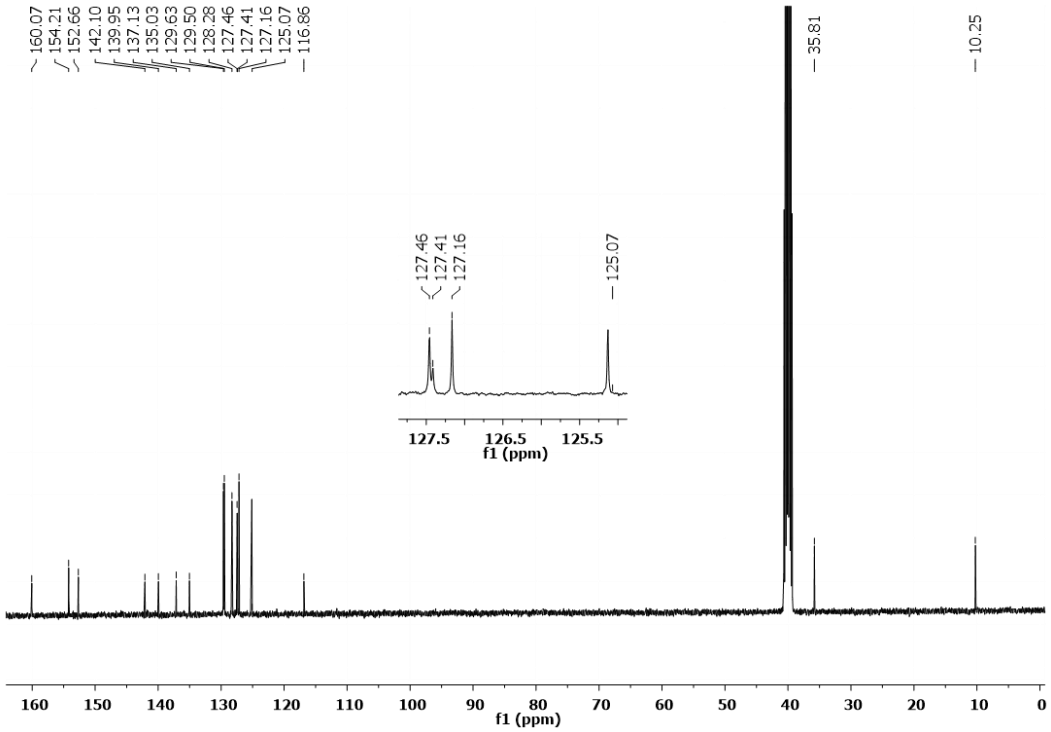

Figure 8 The ^{13}C NMR spectrum in DMSO-d_6 of BiPhAAP

3.5 In vitro antibacterial and antifungal effect

The antimicrobial activity results of BiPhAAP are represented as the zone inhibition percentage in Table 4. When the values are examined, it is seen that this compound has moderate activity against all the selected microorganisms. The results indicate that DMSO alone had no effect on the growth of any of the bacterial and fungi. The test compound BiPhAAP has the highest inhibitory activity at 250, 125 and 62.5 mg/mL for the studied organisms. When the antimicrobial activity was compared to the standard drugs ampicillin and nystatin, we found that BiPhAAP is highly active against *C. albicans* fungi as well as against Gram-positive bacteria *B. subtilis*.

Table 4. Antifungal activity values of BiPhAAP

Concentration (µg/mL)	**Zone of inhibition in mm (ZI) and percentage of inhibition (%)**					
	62.5		**125**		**250**	
	ZI	**%**	**ZI**	**%**	**ZI**	**%**
C. glabrata	10.0±1.0	77	10.0±0.0	71	10.0±0.0	71
A. niger	9.0±1.0	69	10.0±0.0	71	10.0±1.0	71
C. albicans	10.0±1.0	77	9.0±2.0	64	12.0±0.0	86
Nystatin	13.0±3.0	100	14.0±0.0	100	14.0±0.0	100

Table 5. Antibacterial activity values of BiPhAAP

Concentration (µg/mL)	**Zone of inhibition in mm (ZI) and percentage of inhibition (%)**					
	62.5		**125**		**250**	
	ZI	**%**	**ZI**	**%**	**ZI**	**%**
P. vulgaris	12.0±1.0	80	12.0±0.0	75	13.0±1.0	81
E. coli	10.0±0.0	67	10.0±1.0	63	10.0±1.0	63
M. luteus	10.0±0.0	67	9.0±1.0	56	9.0±2.0	56
B. subtilis	12.0±2.0	80	16.0±0.0	100	18.0±1.0	113
Ampicillin	15.0±1.0	100	16.0±1.0	100	16.0±0.0	100

The compound showed these activities at concentration levels of 250 μg/mL for *C. albicans* and 125 and 250 μg/mL for *B. subtilis*. Antimicrobial agents should be in contact with bacterial cells to show their antibacterial potential. Electrostatic attraction, Van der Waals force, receptor–ligand and hydrophobic interactions are some of the contact types. Antimicrobial reagents pass through the bacterial membrane and assemble along the metabolic pathway, affecting the shape and function of the cell wall [48]. The biphenyl ring increases the hydrophobic interactions of the compound by Van der Waals force. These rings increase the lipophilicity of the compound favoring its diffusion along with lipid bilayer of the outer membrane, which is impermeable to most antibacterial agents. Once the compound is inside the bacteria it can interact with proteins, signaling pathways, and biochemical reactions which might prevent cellular proliferation [49, 50].

3.6 Antioxidant effect

The DPPH• is a stable purple color free radical which becomes colorless in reaction with antioxidants. It provides an accurate method to measure the radical scavenging effects of unknown chemicals in comparison to known antioxidants standards such as BHA, BHT, Trolox, and Resorcinol. The BiPhAAP compound showed moderate activity against DPPH• radicals at 5, 25, 50, 100, and 150 μg/mL concentrations (Figure 9a).

According to reducing activity, the Fe^{3+}/ferricyanide complex is reduced to its ferrous form in the presence of an electron donor group. When examined in Figure 9b, the reducing power of BiPhAAP at 150 μg/mL is highest. EDTA and Trolox were studied as standards in evaluating reducing power. The metal chelating activity of BiPhAAP was studied by measuring the inhibition of red-colored Fe^{2+}/ferrozine reagent. Since reactive species transfer an electron to metal, iron cannot induce oxidative damage. Figure 9c shows the metal chelating activity of BiPhAAP. In this method, EDTA, Trolox, and BHT are used as standards. As the concentration increased, the ferrous ion chelating activity of the compound also increased. The highest metal chelating activity of BiPhAAP was observed at 400 μg/mL when compared to the other concentrations used in this research. Superoxide anion scavengers Trolox, BHA, and BHT were used as standards. In this assay, superoxide radicals are generated from the PMS/NADH/O_2 system by reduction of the NBT. Antioxidant compounds inhibit the reduction of NBT. Therefore, we evaluated the antioxidant capacity of BiPhAAP based on its ability to inhibit NBT reduction. It was observed that BiPhAAP as a superoxide anion radical scavenger was as effective as the standards used. Its antioxidant capacity is dose-dependent. As the dose increases its antioxidant activity increases too (Figure 9d).

The reduction of ferric products causes lipid peroxidation. Lipid peroxidation is a marker of oxidative stress. Antioxidant compounds prevent chain reactions by inhibiting lipid peroxidation which the ferrous ions oxidize to the ferric ions in an organism. In this research, we evaluated BiPhAAP ability to prevent lipid peroxidation by using ferric thiocyanate method. In this assay, a linoleic acid emulsion is exposed to oxygen causing the formation of primary and secondary peroxides which in turn causes oxidation of ferrous to ferric thiocyanate. Inhibition of ferric thiocyanate formation by BiPhAAP was measured to evaluate its antioxidant capacity. In this system, high absorbance at the 27th hour points out high linoleic acid emulsion oxidation. Our results showed that BiPhAAP inhibited the formation of ferric thiocyanate more effectively than the standard antioxidants (70.4%) at the same concentration, especially from 25

μg/mL (Figure 10). When the antioxidant activities of the Schiff bases synthesized from the reaction of 4-AAP, and substituted isatins were screened similar results that showed antimicrobial potential were observed [51]. However, no other studies in the literature have been encountered which examine the antioxidant activities of 4-AAP-derived Schiff bases with as many varied tests, as in this work.

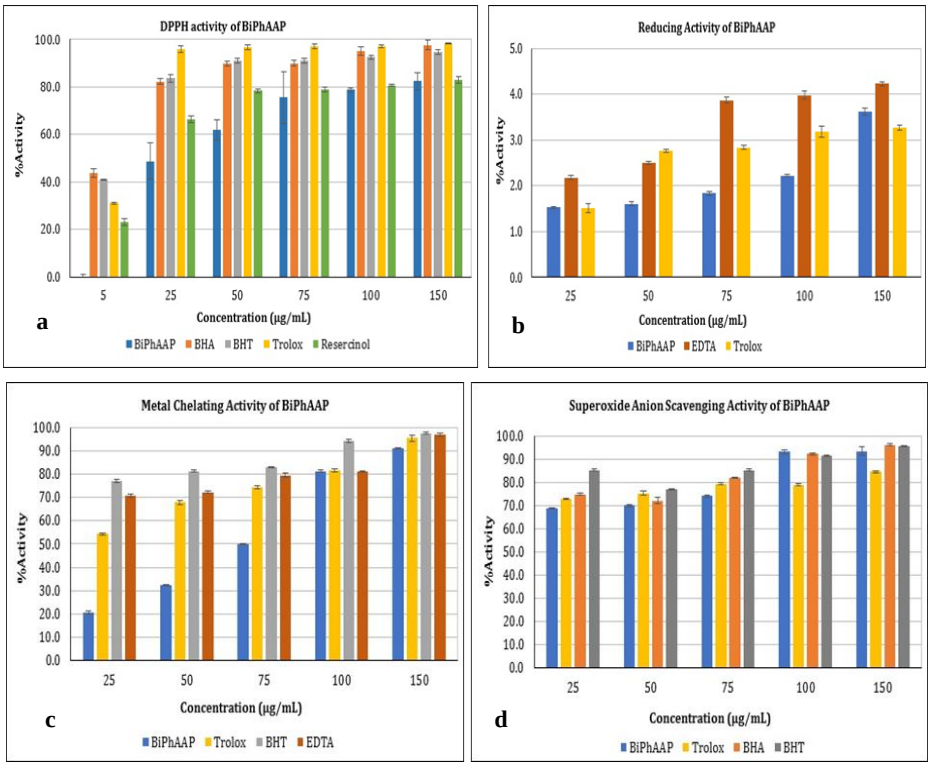

Figure 9. (a) DPPH radical scavenging activity, **(b)** Reducing activity, **(c)** Metal chelating activity, **(d)** Superoxide anion radical scavenging activity of BiPhAAP

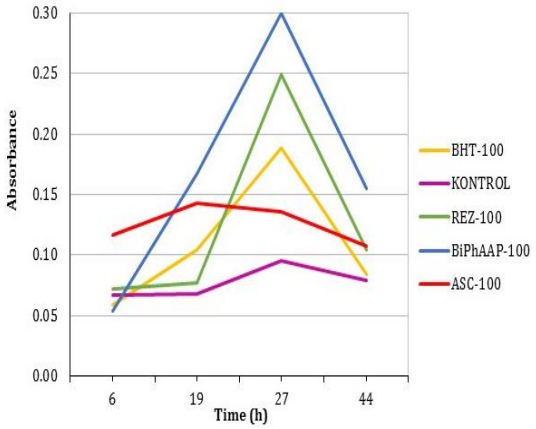

Figure 10. The absorbance of Lipid peroxidation against time (hour) for BiPhAAP (100 µg/mL)

3.7 MTT assay

The cytotoxic effects of BiPhAAP were investigating by using MTT colorimetric cell viability assay on MCF-7 breast carcinoma cells. To measure the dose and time-dependent effect on cell viability, the cells were incubated with increasing concentrations (0-30 mM) of the compound for 24, 48 and 72 hours Analysis of data showed that BiPhAAP has a time and dose cytotoxic effect on MCF-7 breast carcinoma

cells. As the treatment doe and treatment time increase the cell viability decrease (Figure 11).

The IC_{50} (concentration which kills or inhibits cell viability by 50%) value of the compound is shown in Table 6. The IC_{50} values of the tested compound were 7.5, 5.0, and 0.7 mM for 24, 48 and 72 hours, respectively when used against MCF-7 carcinoma cells.

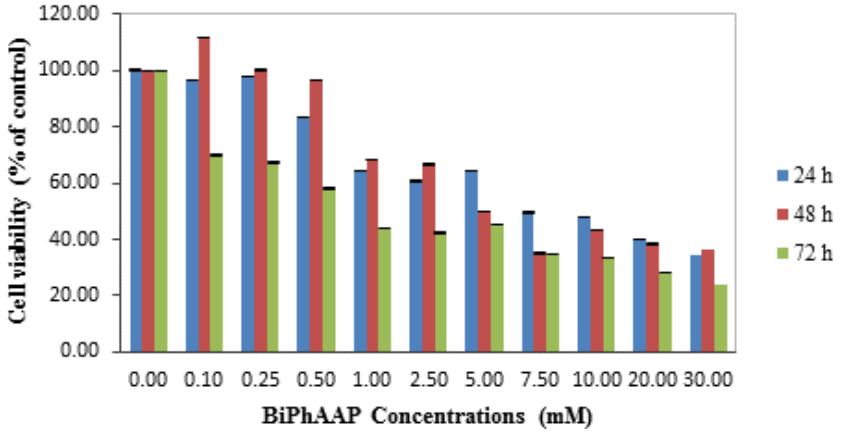

Figure 11. Cell viability of MCF-7 cells after treatment with BiPhAAP for 24h, 48h, 72 h

Table 6. The 50% inhibitory concentrations (IC_{50}) of BiPhAAP for 24, 48, 72 hours

Cell	Time (h)	IC_{50} (mM)
MCF-7	24	7.50±0.40
	48	5.00±0.28
	72	0.70±0.08

It was detected that the cell viability diminished as the concentration of the compound increases. The results of 72 h incubation showed the highest cytotoxic activity. According to Overtone the lipid nature of the cell membrane makes it highly permeable to lipophilic substances, therefore, there is a direct relationship between lipo-solubility, bioavailability, and bioactivity. Furthermore, it increased the delocalization of π-electrons and the lipophilicity. This enhanced lipophilicity presumably causes to decrease the solubility and the permeable barriers of the cell, while in turn promoting both the bioavailability and bioactivity of the molecule [52]. In particular, the effect of the phenyl substituent on cytotoxic activity is well-known. In a study with 2-Acetylpyridine N-substituted thiosemicarbazone ligands and their complexes, it was stated that these compounds had higher activity on MCF-7 breast carcinoma cell lines than cisplatin, the control drug. The researchers concluded that the higher cytotoxic activity in the compounds could originate from the terminal phenyl group in their structure [53, 54]. Therefore, we concluded that the increase the cytotoxic activity of BiPhAAP in our study may be due to the biphenyl ring attached to the 4-AAP skeleton.

4. Conclusion

In conclusion, BiPhAAP (**3**) was synthesized and its structure was analyzed and confirmed by spectroscopy (FT-IR, ^{1}H, and ^{13}C-NMR), elemental analysis, and single crystal X-ray crystallography. All analysis results were in agreement with the proposed Schiff base form. X-Ray crystallography showed that the structure is in the triclinic space group *P*1. Its unit cell parameters are a = 7.126 (3) Å, b = 9.446 (5) Å, c = 15.100 (8) Å, α = 85.15 (4)°, β = 79.74 (4)° and γ = 81.53 (4)°. MHS showed that the compound was propped primary by H···H (56.6%), C···H/H···C (26.5%), O···H/H···O (6.0%) and

N···H/H···N (3.6%) intermolecular interactions. The calculated vibrational frequencies of 0.8929 for HF/6-31G (d) and 0.9613 for B3LYP/6-31G (d) were given with the experimental infrared frequencies. The notable difference observed for the vibrational frequency determined as 32 cm^{-1} and 71 cm^{-1} for the C = O stretching vibrations with regard to B3LYP/6-31G (d) and HF/6-31G (d) methods, respectively, indicates that C–H……O intramolecular hydrogen bond is present in the crystal frame. The in-vitro antimicrobial and antioxidant capacities of the synthesized compound were studied by agar well diffusion method and five different antioxidant capacity methods (DPPH, metal chelating, reducing power, superoxide scavenging, and total antioxidant activity assays). For the title compound, the moderate potential was observed against the bacteria and yeasts. BiPhAAP exhibited higher activity especially for *C. albicans* from fungus and Gram-positive *B. subtilis* from bacteria. Generally, BiPhAAP was as effective as the standards used, by increasing concentration in selected antioxidant activity tests. Based on our MTT results, it can be said that BiPhAAP can restrain the proliferation of MCF-7 cells under the experimental conditions. Therefore, BiPhAAP may be a candidate as an antitumor drug, used alone or in combination with other chemotherapeutics.

Acknowledgment

This research was funded by Ordu University Scientific Research Projects Coordination Department (ODU-BAP) under financial support (No. HD-1709).

References

[1] N. Raman, S. Johnson Raja, and A. Sakthivel, "Transition Metal Complexes with Schiff-Base Ligands: 4-Aminoantipyrine Based Derivatives–A Review," *J. Coord. Chem.*, 62 (5), 691–709, 2009.

[2] M. M. Ghorab, M. G. El-Gazzar, and Mansour S. Alsaid, , "Synthesis, Characterization and Anti-Breast Cancer Activity of New 4-Aminoantipyrine-Based Heterocycles," *Int. J. Mol. Sci*., 15, 7539-7553, 2014.

[3] H. Liang, Q. Yu, R-X. Hu, Z. Y. Zhou, X.G. Zhou, "Synthesis, Crystal Structure and Spectroscopic Properties of a Copper(II) Complex of the Schiff-Base Derived from Picolinaldehyde N-oxide and 4-Aminoantipyridine," *Transit Metal Chem*., 27, 454-457, 2002.

[4] V. C. Filho, R. Correa, Z.Vaz, J. B.Calixto, R. J. Nunes, T. R. Pinheiro, A. D. Andricopulo, R. A. Yunes, "Further Studies on Analgesic Activity of Cyclic Imides," *Farmaco*, 53(1), 55–57, 1998.

[5] V. Prakash, M.S. Suresh, "Preparation Characterization, ^{1}H, ^{13}C NMR Study and Antibacterial Studies of Schiff Bases and Their Zn(II) Chelates," *Res J Pharm Biol Chem Sci.*, 4(4), 1536-1550, 2013.

[6] I. Mohanram, J. Meshram, A. Shaikh, B. Kandpal, "Microwave-Assisted One-Pot Synthesis of Bioactive UGI-4CR using Fluorite as Benign and Heterogeneous Catalyst," *Synth. Commun*," 43, 3322-3328, 2013.

[7] K. Bernardo, S. Leppard, A. Robert, G. Commenges, F. Dehan, B. Meunier, "Synthesis and Characterization of New Chiral Schiff Base Complexes with Diiminobinaphthyl or Diiminocyclohexyl Moieties as Potential Enantioselective Epoxidation Catalysts," *Inorg. Chem*., *35*, 387–396, 1996.

[8] D. Chiaramonte, J. M. Steiner, J. D. Broussard, K. Baer, S. Gumminger, E. M. Moeller, D. A. Williams, R. Shumway, "Use of a ^{13}C-Aminopyrine Blood Test: First Clinical Impressions," *Can. J. Vet. Res*., 67, 183–188, , 2003.

[9] Shamsuzzamana, H. Khanam, A. A., Mashraia, M. Asif, A. Ali, A. Barakat, Y. N. Mabkhot "Synthesis, Crystal Structure, Hirshfeld Surfaces, and Thermal, Mechanical and Dielectrical Properties of Cholest-5-ene," *J. Taibah Univ. Sci*., 11, 141–150, 2017.

[10] M. G. Perez, L. Fourcade, M. A. Mateescu, J. Paquin, "Neutral Red versus MTT Assay of Cell Viability in the Presence of Copper Compounds," *Anal. Biochem*., 535, 43-46, 2017,

[11] E. Apohan, Ü. Yilmaz, Ö.Yilmaz, A.Serindag, H. Küçükbay, Ö. Yesilada, Y. Baran, "Synthesis, Cytotoxic and Antimicrobial Activities of Novel Cobalt and Zinc Complexes of Benzimidazole Derivatives," *J. Organomet. Chem*., 828, 52-58, 2017.

[12] C. Simioni, G. Zauli, A. M. Martelli, M. Vitale, G. Sacchetti, A. Gonelli, L. M. Neri, "Oxidative Stress: Role of Physical Exercise and Antioxidant Nutraceuticals in Adulthood and Aging," *Oncotarget*, 9(24), 17181-17198, 2018.
[13] B. Poljsak, D. Šuput, I. Milisav "Achieving the Balance Between ROS and Antioxidants: When to Use the Synthetic Antioxidants," *Oxid MedCell Longev*., 2013, 1-11, 2013.
[14] Stoe Cie X-AREA (Version1.18) and X-RED32 (Version 1.04), Darmstadt, Germany, 2002.
[15] G. M. Sheldrick, "A Short History of SHELX," *Acta Crystallogr., Sect. A: Found. Crystallogr*., A64, 112–122, 2008.
[16] L. J. Farrugia, "*ORTEP*-3 for Windows - A Version of *ORTEP*-III with a Graphical User Interface (GUI). *J. Appl. Crystallogr*., 30, 565, 1997.
[17] L.J. Farrugia, 1999. "*WinGX* Suite for Small-Molecule Single-Crystal Crystallography," *J. Appl. Cryst*., 32, 837–838.
[18] S.K. Wolff, D.J. Grimwood, J.J., McKinnon, D. Jayatilaka, M.A. Spackman, 2007. CrystalExplorer 2.0, University of Western Australia: Perth, Australia.
[19] H. L. Singh, J. Singh, "Synthesis, Spectroscopic, Molecular Structure, and Antibacterial Studies of Dibutyltin(IV) Schiff Base Complexes Derived from Phenylalanine, Isoleucine, and Glycine," *Bioinorg. Chem. Appl*., 2014, 1-12, 2014.
[20] M. Manjunath, A.D. Kulkarni, G.B., Bagihalli, S. Malladi, S.A. Patil, "Bio-important Antipyrine Derived Schiff Bases and Their Transition Metal Complexes: Synthesis, Spectroscopic Characterization, Antimicrobial, Anthelmintic and DNA Cleavage Investigation," *J. Mol. Struct*. 1127, 314-321, 2017.
[21] W. Brand-Williams, M.E. Cuvelier, C. Berset, "Use of a Free Radical Method to Evaluate Antioxidant Activity," *LWT-Food Sci. Technol*., 28, 25-30, 1995.
[22] M. Oyaizu, 1986. "Studies on Product of Browning Reaction Prepared from Glucose Amine," *Japan Journal of Nutrition*, 44, 307-315.
[23] E. A. Decker, B. Welch, 1990. "Role of Ferritin as a Lipid Oxidation Catalyst in Muscle Food. *J. Agr. Food Chem*.," 38, 674-677.
[24] F. Liu, V.E., Ooi, S.T. Chang, "Free Radical Scavenging Activity of Mushroom Polysaccharide Extracts," *Life Sci.*, 60, 763-771, 1997.
[25] L.W., Chang, W.J. Yen, S.C. Huang, P. D. Duh, "Antioxidant Activity of Sesame Coat," *Food Chem*., 78, 347-354, 2002.
[26] T. Mosmann, 1983. "Rapid Colourimetric Assay for Cellular Growth and Survival: Application to Proliferation and Cytotoxicity Assays," *J. Immunol. Methods*, 65(1-2), 55-63.
[27] S.W. Lim, H.S. Loh, K.N. Ting, B.T. Dawn, Z.N. Allaudin, "Reduction of MTT to Purple Formazan by Vitamin E Isomers in the Absence of Cells," *Trop. Life Sci. Res*., 26(1), 111–120, 2015.
[28] A.D. Becke, "Density- Functional Thermochemistry. III. The Role of Exact Exchange," *J. Chem. Phys*., 98, 5648–5652, 1993.
[29] C. Lee, W. Yang, R.G. Parr, "Development of the Colle-Salvetti Correlation-Energy Formula into a Functional of the Electron Density," *Phys. Rev. B*, 37, 785–789, 1988.
[30] H.B. Schlegel, "Optimization of Equilibrium Geometries and Transition Structures," *J. Comput. Chem*., 3, 214–218, 1982.
[31] C. Peng, P.Y. Ayala, H.B., Schlegel, M.J. Frisch, "Using Redundant Internal Coordinates to Optimize Equilibrium Geometries and Transition States," *J. Comput. Chem*., 17, 49–56, 1996
[32] Frisch, M. J., Trucks, G. W., Schlegel, H. B., Scuseria, G. E., Robb, M. A., Cheeseman, J. R., Montgomery, J. A. Jr, Vreven, T., Kudin, K. N., Burant, J. C., Millam, J. M., Iyengar, S. S., Tomasi, J., Barone, V., Mennucci, B., Cossi, M., Scalmani, G., Rega, N., Petersson, G. A., Nakatsuji, H., Hada, M., Ehara, M., Toyota, K., Fukuda, R., Hasegawa, J., Ishida, M., Nakajima, T., Honda, Y., Kitao, O., Nakai, H., Klene, M., Li, X., Knox, J. E., Hratchian, H. P., Cross, J. B., Bakken, V., Adamo, C., Jaramillo, J., Gomperts, R., Stratmann, R. E., Yazyev, O., Austin, A. J., Cammi, R., Pomelli, C., Ochterski, J. W., Ayala, P. Y., Morokuma, K., Voth, G. A., Salvador, P., Dannenberg, J. J., Zakrzewski, V. G., Dapprich, S., Daniels, A. D., Strain, M. C., Farkas, O., Malick, D. K., Rabuck, A. D., Raghavachari, K., Foresman, J. B., Ortiz, J. V., Cui, Q., Baboul, A. G., Clifford, S., Cioslowski, J., Stefanov, B. B., Liu, G., Liashenko, A., Piskorz, P., Komaromi, I., Martin, R. L., Fox, D. J., Keith, T., Al- Laham, M. A., Peng, C. Y., Nanayakkara, A., Challacombe, M., Gill, P. M. W., Johnson, B., Chen, W., Wong, M. W., Gonzalez, C. & Pople, J. A. (2004). GAUSSIAN03, Gaussian Inc., Wallingford, CT, USA.
[33] R. Dennington, T. Keith, J. Millam, 2007. GaussView4.1. Semichem Inc., Shawnee Mission, KS, USA.
[34] M.J. Turner, J.J. MacKinnon, S.K. Wolff, D.J. Grimwood, P.R. Spackman, D. Jayatilaka, and M. A. Spackman, "Crystal Explorer17.5. University of Western Australia, 2017.

[35] P. Sen, S. Kansiz, N. Dege, T.S., Iskenderov, S.Z. Yildiz, "Crystal Structure and Hirshfeld Surface Analysis of 4-[4-(1H-benzo[d]imidazol-2-yl)phenoxy]phthalonitrile Monohydrate," *Acta Crystallogr., E: Crystallographic Communications*, 74, 994–997, 2018.
[36] E. Aydemir, S. Kansiz, M.K. Gumus, N.Y. Gorobets, N. Dege, "Crystal Structure and Hirshfeld Surface Analysis of 7-Ethoxy-5-methyl-2-(pyridin-3-yl)-11,12-dihydro-5,11-methano-[1,2,4]triazolo[1,5-*c*][1,3,5] benzoxadiazocine," *Acta Crystallographica Section E: Crystallographic Communications*, 74, 367–370, 2018.
[37] S. Kansiz, Z.M. Almarhoon, N. Dege, "Synthesis, Crystal Structure and Hirshfeld Surface Analysis of Tetraaquabis (isonicotinamide-κN1) cobalt (II) fumarate," *Acta Crystallographica Section E: Crystallographic Communications*, 74, 217–220, 2018.
[38] M. K. Gümüş,, S. Kansız, E. Aydemir, N. Y. Gorobets, N. Dege, "Structural Features of 7-Methoxy-5-methyl-2-(pyridin-3-yl)-11,12-dihydro-5,11-methano[1,2,4]triazolo[1,5-c][1,3,5]benzoxadiazocine Experimental and Theoretical (HF and DFT) Studies, Surface Properties (MEP, Hirshfeld)," *J. Mol. Struct*., 1168, 280–290, 2018.
[39] Y. Ünver, K. Sancak, H. Tanak, İ. Değirmencioğlu, E. Düğdü, M. Er, Ş. Işık, "5-Benzyl-4-[3-(1H-imidazol-1-yl) propyl]-2H-1, 2, 4-triazol-3 (4H)-ones: Synthesis, Spectroscopic Characterization, Crystal Structure and a Comparison of Theoretical and Experimental IR Results by DFT Calculations," *J. Mol Struct*., 936(1-3), 46-55, 2009.
[40] J.P. Merrick, D. Moran, L. Radom, "An Evaluation of Harmonic Vibrational Frequency Scale Factors," *J. Phys. Chem. A*, 111, 11683-11700, 2007.
[41] H. Tanak, F. Erşahin, Y. Köysal, E., Ağar, S. Işik, M. Yavuz, "Theoretical Modeling and Experimental Studies on N-n-Decyl-2-oxo-5-nitro-1-benzylidene-methylamine," *J. Mol. Model*., 15(10), 1281-1290, 2009.
[42] H. Gokce, S., Bahceli, "Analysis of Molecular Structure, Spectroscopic Properties (FT-IR, Micro-Raman and UV–vis) and Quantum Chemical Calculations of Free and Ligand 2-Thiopheneglyoxylic acid in Metal Halides (Cd, Co, Cu, Ni and Zn)," *Spectrochim. Acta A: Mol. Biomol. Spectroscop*., 116, 242–250, 2013.
[43] G. Socrates, 2004. "Infrared and Raman Characteristic Group Frequencies. John Wiley & Sons. NewYork, London, 362s.
[44] J. Joseph, G.A.B. Rani, "Metal-Based Molecular Design Tuning Biochemical Behavior: Synthesis, Characterization, and Biochemical Studies of Mixed Ligand Complexes Derived From 4-Aminoantipyrine Derivatives," *Spectroscop. Lett*., 47(2), 86-100, 2014.
[45] N. Raman, J. D., Raja, A. Sakthivel, "Synthesis, Spectral Characterization of Schiff Base Transition Metal Complexes: DNA Cleavage and Antimicrobial Activity Studies," *J. Chem.Sci.,* 119(4), 303–310, 2007.
[46] V. Srinivasan, H. Sivaramakrishnan, B. Karthikeyan, "Detection, Isolation and Characterization of Principle Synthetic Route Indicative Impurity in Telmisartan," *Arab. J. Chem*., 9(2), 1516-1522, 2016.
[47] M.A. Hadi, "Coordination Behavior of N/O Donor Ligand with Some Transition Metals," *Acta Chimica Pharmaceutica Indica*, 3(2), 127-134, 2013.
[48] L. Wang, C. Hu, L. Shao "The Antimicrobial Activity of Nanoparticles: Present Situation and Prospects for the Future," *Int. J. Nanomedicine*, 2017(12), 1227–1249, 2017.
[49] Z.H., Chohan, A. Scozzafava, C.T. Supuran, "Zinc Complexes of Benzothiazole-Derived Schiff Bases with Antibacterial Activity," *J. Enzyme Inhib. Med. Chem*., 18(3), 259-263, 2003.
[50] J. Joseph, G.A.B. Rani, "Antioxidant and Biochemical Activities of Mixed Ligand Complexes," *Appl. Biochem. Biotechnol*., 172(2), 867–890, 2014.
[51] T. Gabriela, D.S. Catalina, Z. Ana-maria, J. Alexandra, T. Cristina, 2014. "Preliminary Screening of Biological Activities of Some new Schiff Bases of Isatins," *Farmacia*, 62(1), 14-22.
[52] Z. Uyar, D. Erdener, İ. Koyuncu, Ü. Arslan, 2017. "Synthesis, Characterization, and Cytotoxic Activities of a Schiff Base Ligand and Its Binuclear Copper(II) and Manganese(III) Complexes," *J. Turkish Chem. Soc., Sect. Chem*., 4(3), 963-980.
[53] N. A. Taş, A. Şenocak, A. Aydın,. "Preparation and Cytotoxicity Evaluation of Some Amino Acid Methyl Ester Schiff Bases," *J. Turkish Chem. Soc., Sect. Chem*, 5(2), 585-606, 2018.
[54] R. Manikandan, P. Viswanathamurthi, K. Velmurugan, "Synthesis, Characterization and Crystal Structure of Cobalt(III) Complexes Containing 2-Acetylpyridine thiosemicarbazones: DNA/Protein Interaction, Radical Scavenging and Cytotoxic Activities," *J. Photoch. Photobio. B*., 130, 205–216, 2014.